Available online at www.sciencedirect.com
SCIENCE DIRECT®
Journal of Power Sources 145 (2005) 353–361
JOURNAL OF POWER SOURCES
www.elsevier.com/locate/jpowsour

Analyses of the fuel cell stack assembly pressure

Shuo-Jen Lee*, Chen-De Hsu, Ching-Han Huang

Department of Mechanical Engineering, Yuan Ze University, 135 FarEast Road, NeiLi, TaoYuan, Taiwan, ROC

Accepted 3 February 2005
Available online 20 April 2005

Abstract

A proper stacking design and cell assembly are important to the performance of fuel cells. The cell assembly will affect the contact behavior of the bipolar plates with the membrane electrode assembly (MEA). Not enough assembly pressure may lead to leakage of fuels, high contact resistance and malfunctioning of the cells. Too much pressure, on the other hand, may result in damage to the gas diffusion layer and/or MEA. The stacking design may affect the pressure distribution within the fuel cell stack and thus the interfacial contact resistance. Uneven distribution of the contact pressure will result in hot spots which may have a detrimental effect on fuel cell life.

In this study, finite element analysis (FEA) procedures were established for a PEM single cell with point stack assembly method. The mechanical properties and geometrical dimensions of all the fuel cell components, such as bipolar plates, membrane, gas diffusion layer and end plates were collected for accurate simulation. From the FEAs, the compliance as well as the pressure distribution of the single cell was calculated. In order to verify the results of the analysis, experimental tests, with a pressure film inserted between the bipolar plates and the MEA, were conducted to establish the actual pressure distribution. Color variations of the pressure film could be calibrated to obtain pressure distribution. Compliance of the gas diffusion layer was also measured. The analysis procedures for the fuel cell stacking assembly were established by comparing the simulation results with those of the experimental data at various levels of assembly pressures. They can help determine the proper stacking parameters such as stacking design, bipolar plate thickness, sealing size and assembly pressure, and are important in obtaining a consistent fuel cell performance.

Keywords: Stack assembly; Assembly pressure; Gas diffusion layer; MEA; Pressure distribution; Compliance; FEM analysis

1. Introduction

The stacking design and cell assembly parameters significantly affect the performance of PEM fuel cells. The dedicated integral micro-porous structures and brittle mechanical properties of the gas diffusion layer and the MEA should be preserved as much as possible after cell assembly. For example, the assembly pressure affects the characteristics of the contact interfaces between components. Insufficient assembly pressure may result in sealing problems, such as fuel leakage, internal combustion and un-acceptable contact resistance. On the other hand, too much pressure may damage the MEA and the gas diffusion layer, resulting in a broken porous structure and a blockage of the gas diffusion passage. In both cases, it will decrease the cell performance.

Lee et al. [1] measured the cell performance of PEM fuel cells with different, commercially available, gas diffusion layers under various assembly pressures. They found that each gas diffusion layer had its own optimal assembly pressure due to differences in mechanical properties and micro-porous characteristics. Chu [2] proposed a mathematical model for the porous structure of the PEM gas diffusion layer and its effects on cell performance.

Because of the relatively thin dimensions and low mechanical strength of the gas diffusion layer and MEA versus sealant, bipolar plates and end plates, the most important goal in the stack design and assembly is to achieve a proper and uniform pressure distribution. In order to achieve a uniform pressure distribution, many stacking designs have been proposed [3–5]. Zhang [6] employed hydro-pressure on the end

* Corresponding author. Tel.: +886 3 4648800; fax: +886 3 4558013.
E-mail address: mesjl@saturn.yzu.edu.tw (S.-J. Lee).

0378-7753/$ – see front matter © 2005 Elsevier B.V. All rights reserved.
doi:10.1016/j.jpowsour.2005.02.057

plates in order to obtain uniform pressure. He demonstrated that the cell performed better than the traditional nut and bolt point-load stacking design. However, there are few reports on the simulation of the cell assembly and experimental measurements.

2. Goals and methodology

The goal of this research was to propose a methodology and a FEA simulation procedure for establishing numerical tools for the evaluation of the stacking design and cell assembly parameters. From the numerical simulation, the methods of stacking design, the critical dimensions and material selection of fuel cell components, and assembly pressure were investigated for the purpose of achieving a consistent cell performance. The schematic plot of the methodology is shown in Fig. 1. It is composed of a numerical simulation and the experimental verification. From the experimental measurement, the numerical model and the assumptions were verified for further design evaluation and parametric studies.

The well-established finite element method was employed for the numerical simulation of the mechanical responses (stress, strain and compliance) of the cell assembly. First, the dimensions and mechanical properties of all fuel cell components were collected. Fig. 2 shows the stacking sequence and components of the single cell in this study. The type and amount of assembly pressure depends on the type of stacking designs. In general, they can be categorized into three types: point load-design, line-load design and surface-load design. The traditional point-load design with several bolt and nut assemblies is shown in Fig. 2. The amount of assembly pressure depends on the geometrical shape of the end plate, and on the dimensions and physical properties of all the fuel cell components. To-date it always has been determined by the trial-and-error process. Boundary conditions and the behavior of the contacting interface of the components must be consistent with the actual physical situation. Finally, the proper types of element for each component and their interfaces must be selected so as to allow a realistic physical behavior. Meshing is also important for an accurate result. The significant difference in thickness between the components requires special consideration in the meshing scheme. The simulated results of stress, strain, pressure distribution and the compliance contours for each component must be plotted for detailed evaluation, so that the effects of the design variables and process parameters on the cell assembly can be quantified.

In order to verify the numerical model and modeling assumptions, actual experiments were conducted to measure the pressure distribution of the MEA, and the compliance of the gas diffusion layer for each assembly pressure. The pressure distribution was measured by means of a pressure film. The compliance was measured by micrometer. The results were compared with those of the numerical simulation. After experimental verification, the established numerical simula-

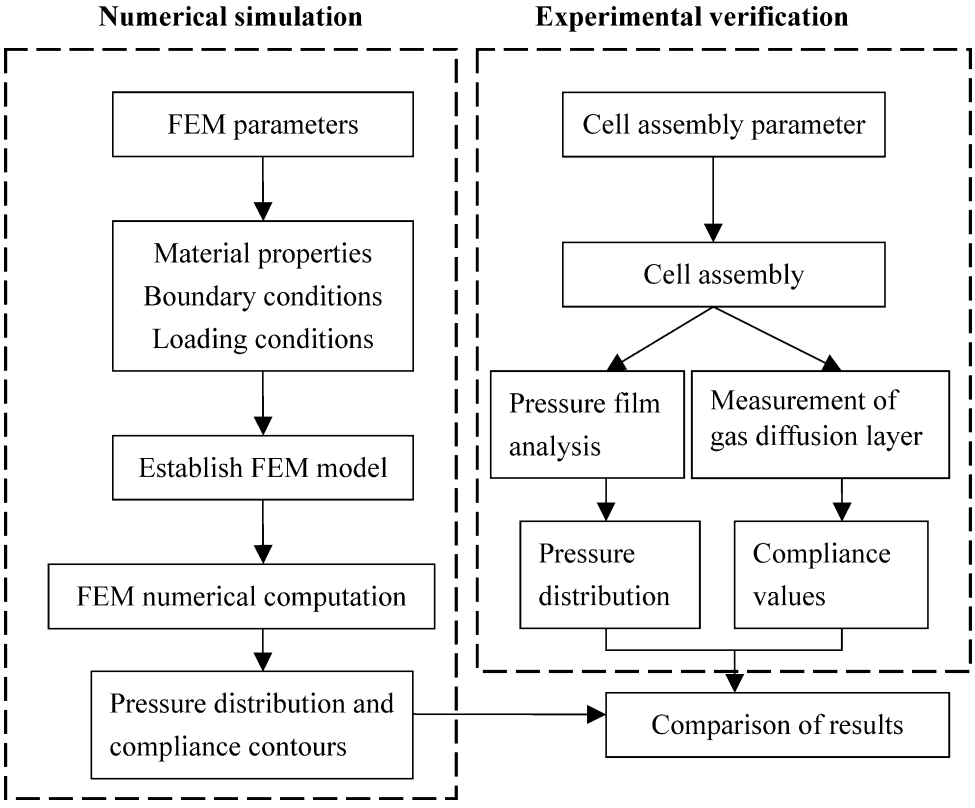

Fig. 1. Schematic plot of the simulation methodology.

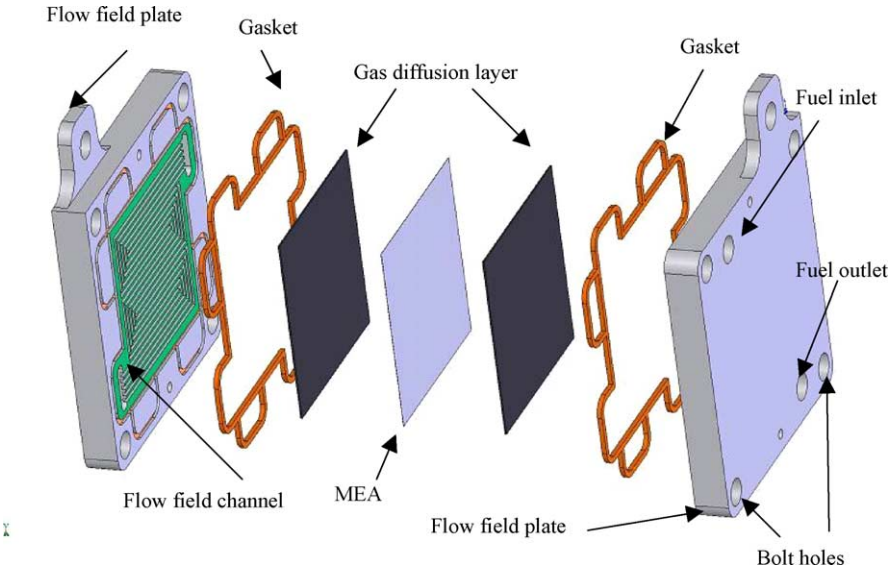

Fig. 2. Components and stacking sequence of the single cell for modeling.

tion procedures can be used to evaluate a new stacking design and/or optimize cell assembly parameters.

3. Numerical simulation

The PEM fuel cell is composed of several components. The contact behavior between these components is highly non-linear. A simple but effective contact model is essential for representing the actual physical phenomena with a realistic numerical model. The well-established finite element analysis was employed for the numerical simulation. The commercial code of ANSYS was used in this study.

3.1. FEA structural model

The components of a fuel cell consist of end plates, bipolar plates, sealants, gas diffusion layers and MEA. In this study, a single cell was designed for numerical simulation and experiments. The flow field plate integrated the functions of the end plates for mechanical strength, the current conducting plate for current collection, and the bipolar plates for flow field channel, as shown in Fig. 2. The flow field plate was fabricated from Al 5052, and measured 84 mm × 84 mm × 10 mm. The flatness form error was about ±0.02 mm. The flow field channel was 1.2 mm wide by 1.0 mm deep. A polymer gasket, about 0.8 ± 0.08 mm diametre in cross-section, acted as the sealant to prevent fuel leakage. The effective fuel cell area was 50 mm × 50 mm. The gas diffusion layer was a 0.5 ± 0.03 mm thick carbon paper. It was brittle and had a micro-porous structure. The MEA was a three-layered structure with a Nafion 112 membrane, and was only 0.05 mm in thickness.. The dimensions and mechanical properties of above components are listed in Table 1.

It is apparent from Table 1 that the elasticity modulus of the flow field plate, 70,000 kgf mm^{-2}, was much higher than that of the other components. The MEA had the smallest elastic modulus, 1.85 kgf mm^{-2}. However, it was thin and elastic and therefore may endure a certain amount of deformation. It can deform with the gas diffusion layer or the flow field plate. The gasket is elastic, and its thickness is slightly more than the gas diffusion layer. It is intended to ensure fuel sealing. It can absorb some form error as well as manufacturing tolerance of the fuel cell components. Therefore, the critical component was the gas diffusion layer due to its property of being brittle. As the gasket becomes compressed by the assembly pressure, it will accommodate the flatness error of the flow field plate as well as its own manufacturing tolerance. Then, it will compress the gas diffusion layer. If not enough pressure is applied, it may not

Table 1
Dimensions and mechanical properties of single cell components

Component	Material	Modulus of elasticity (kgf mm^{-2})	Poisson's ratio	Size (mm)	Manufacturing tolerance (thickness) (mm)
Flow field plate	Al 5052	70000	0.29	84 × 84 × 10	±0.02
Gas diffusion layer	Carbon paper	5.745	0.33	5 × 5 × 0.5	±0.03
MEA	Nafion 112	1.85	0.33	5 × 5 × 0.05	
Gasket	VMQ	55	0.3	ϕ = 0.8	±0.08

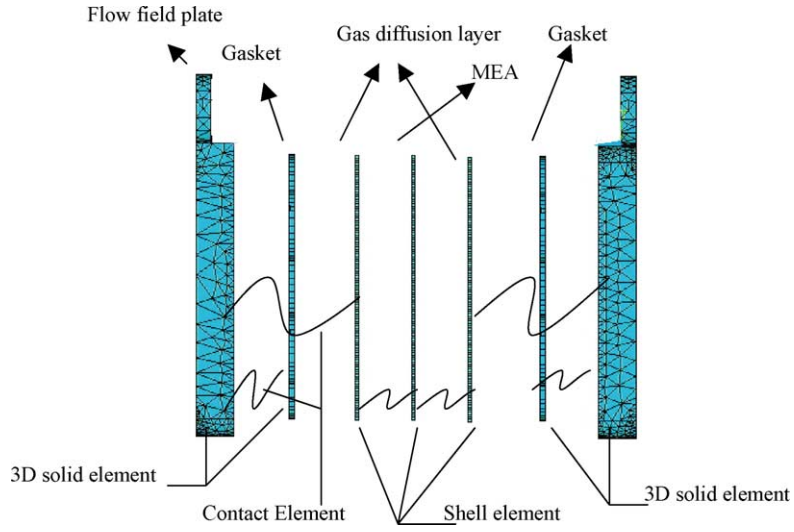

Fig. 3. Finite element model of the single cell.

ensure sufficient contact between the flow field plate, gas diffusion layer and the MEA. However, the brittle gas diffusion layer can be damaged if too much pressure is applied.

3.2. The finite element model

The proper finite element type must be selected to represent the physical behavior of each component and their interfaces. Because both the gas diffusion layer and the MEA are thin, the shell element with six degrees of freedom was selected. The 3D solid element was used to represent the flow-field plate and the gasket. In order to model the contact behavior, the contact elements were connected between the gas diffusion layer and the MEA, the gas diffusion layer and the flow-field plate, and between the gasket and the flow-field plate. A combination of mapped meshing and automatic meshing was adopted in order to ensure proper element con-

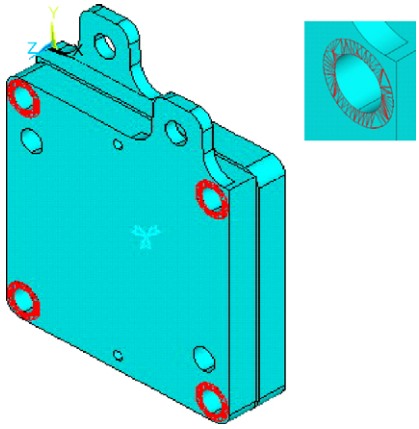

Fig. 4. Loading conditions of the finite element model.

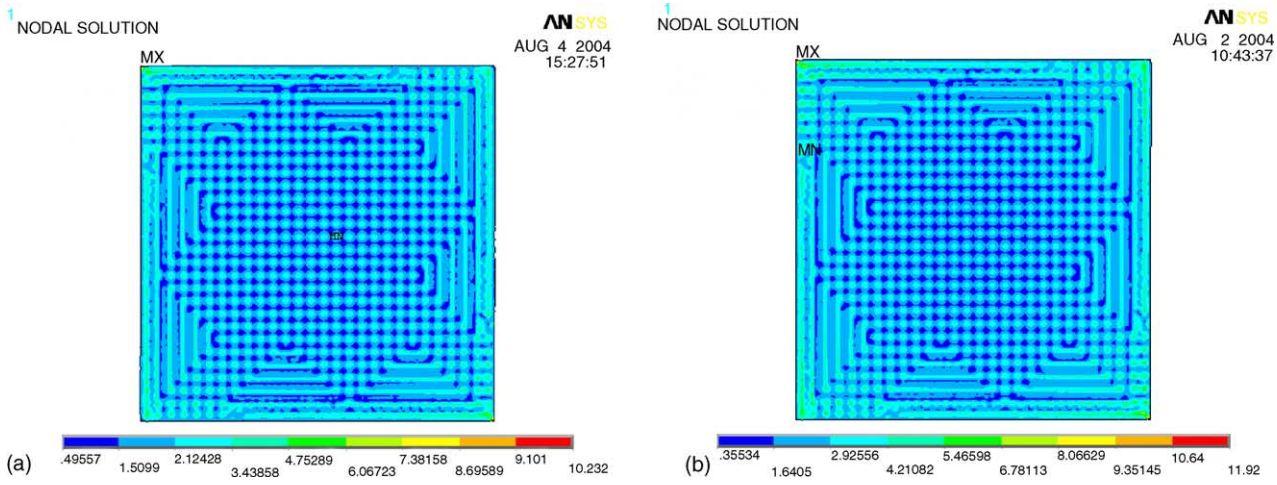

Fig. 5. Simulated pressure distribution plots of the MEA assembly: (a) 15 kgf mm^{-2} and (b) 25 kgf mm^{-2}.

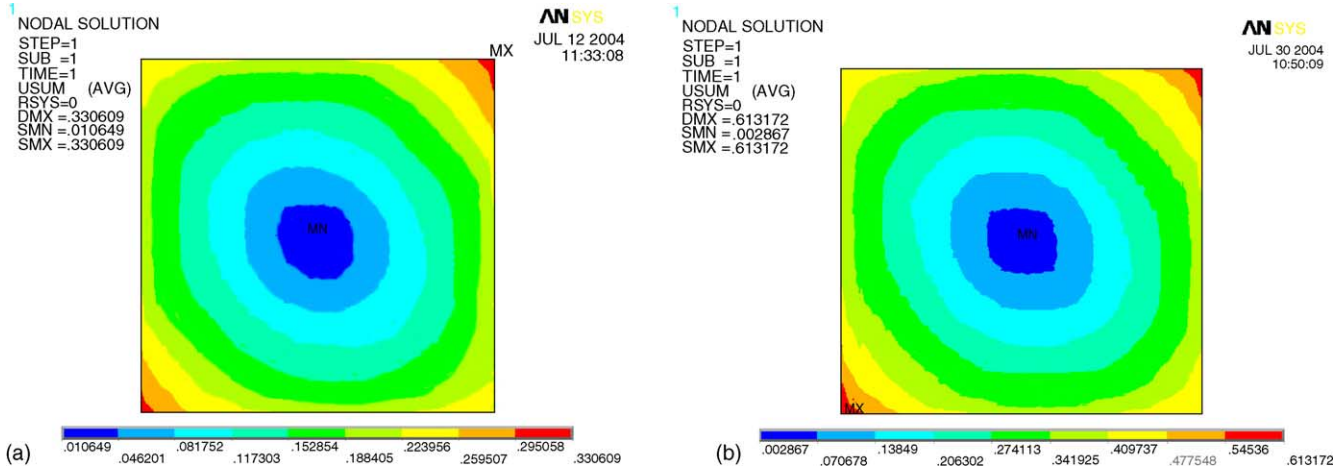

Fig. 6. Simulated compliance plots of the gas diffusion layer: (a) 15 kgf mm^{-2} and (b) 25 kgf mm^{-2}.

nectivity and a correct aspect ratio. Fig. 3 shows the finite element model of the single cell.

3.3. Boundary and loading conditions

The assembly pressure was applied through four bolt and nut assemblies at the corners. To simplify the numerical model, the bolts and nuts were ignored in the finite element model. The assembly pressure was applied directed at the contacting areas of both flow field plates as shown in Fig. 4. The finite element model had to be properly constrained in order to prevent free movement. Assuming that the model was symmetric in the middle plane, the degree of freedom of the contact elements between top and bottom gasket were assumed to be zero. This does not affect the compliance behavior of the gas diffusion layers and the gasket (Fig. 4).

3.4. Simulation results

Four loading conditions were simulated, with a cell assembly pressure of 15, 20, 25, and 30 kgf mm^{-2}, respectively. The results of the MEA pressure distribution and the gas diffusion layer compliance are shown in Fig. 5(a) and (b) and present the simulated pressure distribution plots of the MEA for cell assembly pressure of 15 and 25 kgf mm^{-2}. These figures demonstrate that the imprint marks of the two perpendicularly oriented flow field channels are not clear when the pressure is low. However, the imprint mark becomes very clear when the assembly pressure reaches 25 kgf mm^{-2}. The pressure values ranged from 1.51 to 3.49 kgf mm^{-2} and from 1.64 to 4.21 kgf mm^{-2} for both cell assembly pressures of 15 and 25 kgf mm^{-2}, respectively. Fig. 5(a) and (b) also show that the pressures were higher at the four corners and lower towards the center.

The simulated compliance contours of the gas diffusion layer are shown in Fig. 6(a) and (b) for the assembly pressures of 15 and 25 kgf mm^{-2}. The range of compliance was from 0.105 to 0.336 mm and from 0.002 to 0.613 mm, respectively. The contours were slightly non-symmetric due the non-symmetric nature of the top and bottom flow-field plates. Fig. 6(a) shows that the compliance at the center was

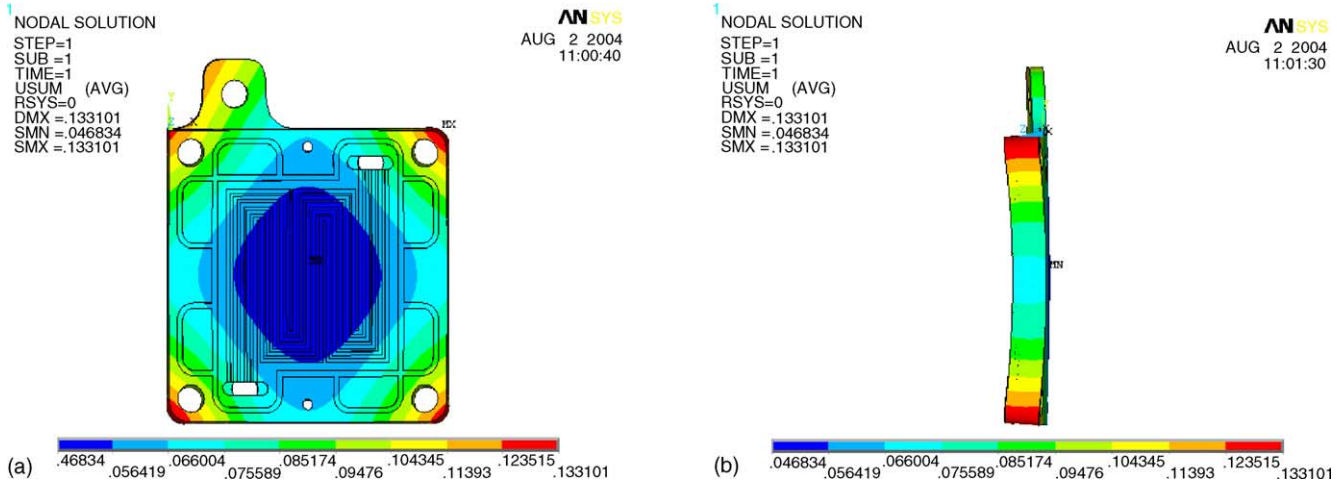

Fig. 7. Deformation contours of the flow field plate under 25 kgf cm^{-2}: (a) front view and (b) side view.

Table 2
Simulated pressure values of the MEA

Assembly pressure (kgf mm^{-2})	Simulated pressure at various locations (kgf mm^{-2})								
	1	2	3	4	5	6	7	8	9
15	2.01	1.47	2.17	1.44	0.59	1.45	2.25	1.48	2.08
20	2.25	1.55	2.29	1.66	0.68	1.46	2.33	1.67	2.15
25	5.46	3.12	5.55	2.83	1.25	2.91	5.98	2.71	5.88
30	8.56	5.21	8.55	4.72	2.01	5.01	8.68	4.56	8.43

Table 3
Simulated compliance values of the gas diffusion layer

Assembly pressure (kgf mm^{-2})	Simulated compliance at various locations (mm)								
	1	2	3	4	5	6	7	8	9
15	0.062	0.044	0.059	0.047	0.009	0.039	0.061	0.049	0.071
20	0.113	0.091	0.137	0.102	0.028	0.092	0.144	0.099	0.125
25	0.152	0.128	0.178	0.134	0.032	0.119	0.172	0.138	0.157
30	0.178	0.155	0.179	0.162	0.040	0.149	0.179	0.163	0.177

almost zero. The contours of Fig. 6(b) were more definitive. Both figures show that the compliances were larger at the four corners and smaller at the center.

In order to verify the effects of the point load stacking design on the pressure distribution as well as on the compliance contours, the deformation plots of the flow field plate are shown in Fig. 7(a) and (b) for the assembly pressure of 25 kgf mm^{-2}. Fig. 7(a) clearly shows that the deformation was larger at the four corners where the pressure was applied. And then it dropped considerable toward the center creating a non-uniform distribution. This method of stack assembly is in-effective and not recommended for uniform pressure distribution. The diamond-shaped contour instead of a round contour indicates that the flow field channel had affected the strength of the flow-field plate. Fig. 7(b) also shows that the plate was bent. The maximum deformation was about 0.133 mm.

Values at nine locations of both the gas diffusion layer and the MEA, see Fig. 8, are shown for further comparison. From the contour plots, the values at locations 1, 3, 7, and 9 are expected to be higher while at location 5—the center will be the lowest. The pressure values of the MEA at the nine locations, under the four assembly pressures, are listed in Table 2. The pressure value under the assembly pressure of 15 kgf mm^{-2} is about 2.1 kgf mm^{-2} (14%) at the four corner locations of 1, 3, 7, and 9. At the center, location 5, the pressure value is only 0.59 kgf mm^{-2} (4%). At 25 kgf mm^{-2} assembly pressure, the percentage pressure at the corner locations is about 22% and about 5% at the center. The variation in pressure distribution was large. Although the mechanical strength of the aluminum flow field plate, as shown in Table 1, was much higher than the other components, the results show that the point load stacking design is not a good method for obtaining a uniform pressure distribution.

Table 3 lists the simulated compliance values of the gas diffusion layer. At 15 kgf mm^{-2}, the compliance value was about 0.062 mm at the corner locations and only 0.009 mm at the center. This means that the center location was only touching the flow field plate. This may result in a larger contact resistance. At 25 kgf mm^{-2}, the compliance value at the center was about 0.032 mm, or about 6% of the original thickness of 0.5 mm. However, it was about 0.17 mm, or 34% of the original thickness, at the corners. The contact in the center may be correct, but it was reaching the limit of damaging the micro-porous structure of the gas diffusion layer.

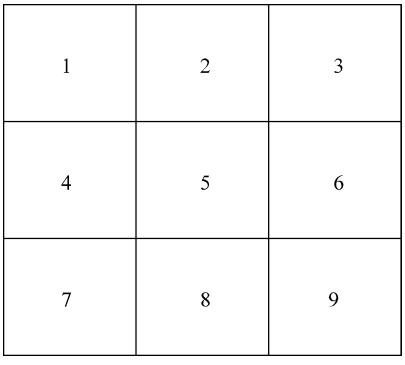

Fig. 8. Locations for numerical comparison.

4. Experimental verification

In order to verify the above simulation results, experiments were conducted to measure the pressure distribution of the MEA, and the compliance of the gas diffusion layer. A single cell, same as the numerical model, was built for testing, see Fig. 2. The dimensions of the cell components are listed in Table 1. The form error of the flow-field plate and the manufacturing tolerances of the other components are also listed in Table 1. The flatness error of the flow field plate was ±0.02 mm. The variation of gasket diameter was about ±0.01 mm. The variation in gas diffusion layer thickness was about ±0.01 mm.

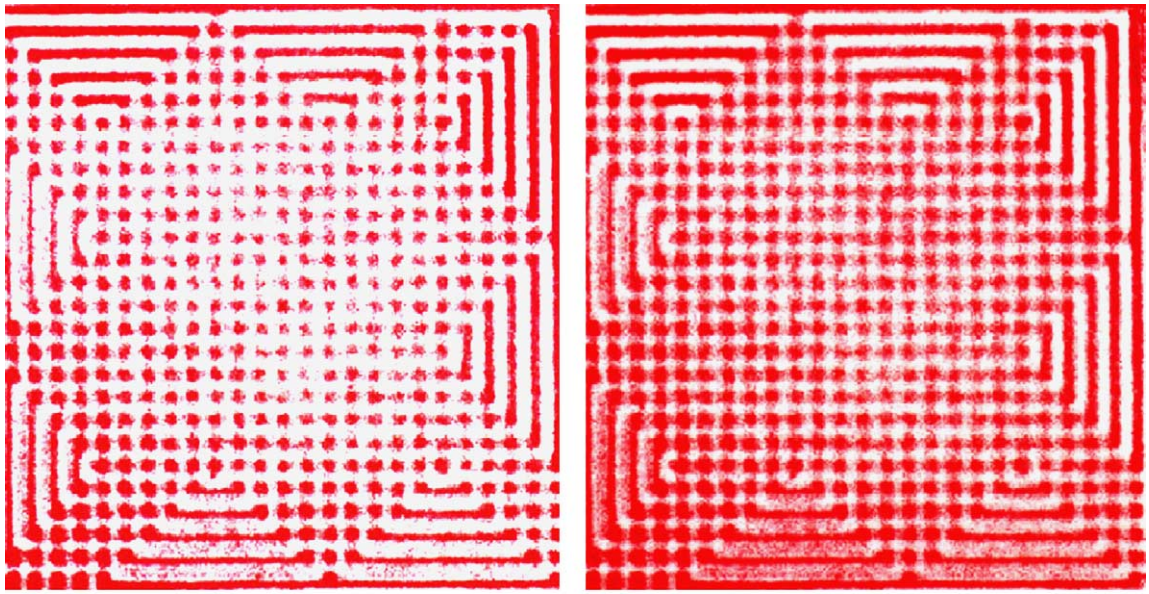

Fig. 9. Measured pressure distribution contours from the pressure film: (a) 15 kgf mm^{-2} and (b) 25 kgf mm^{-2}.

Measurements were taken at location of Fig. 8. Four tests with cell assembly pressures of 15, 20, 25, and 30 kgf mm^{-2} were conducted. Their values were recorded and compared with those of the numerical simulation data.

4.1. The measurement methods

A Fuji pre-scale pressure film replaced the MEA during the test. Color transformation takes place when the pressure film is being compressed. The color transformed pressure film is then transferred into an image file by scanning. The image file is then compared with the reference color bar to obtain the pressure value. However, it was found that the color bar was not sensitive enough to provide an accurate pressure distribution. Therefore, a Matlab file was written to transfer the color image file into a gray level image file. This proved to be more effective in providing the quantified pressure distribution contours.

The compliance of the gas diffusion layer was measured by micrometer at the nine locations of Fig. 8.

4.2. The experimental results

Fig. 9(a) and (b) show the measured pressure distribution of the MEA at 15 and 25 kgf mm^{-2} cell assembly pressure. The image of Fig. 9(a) is very light meaning that the pressure level was low in general. The imprint mark of the flow field channel was sparse and vague. This indicated that the MEA was not in full contact with both the gas diffusion layer and the flow field plate. The image of Fig. 9(b) was clearer

Table 4
Measured pressure values from the pressure film

Assembly pressure (kgf mm^{-2})	Measured pressure at various locations (kgf mm^{-2})								
	1	2	3	4	5	6	7	8	9
15	1.78	1.25	1.65	1.26	0.83	1.03	1.55	1.05	1.77
20	3.15	1.92	2.98	2.33	1.08	2.36	3.33	2.26	3.56
25	4.71	2.54	4.08	2.75	1.55	2.39	3.95	2.37	4.31
30	5.21	4.47	5.44	5.56	2.55	4.45	5.36	5.58	5.23

Table 5
Measured compliance values of the gas diffusion layer

Assembly pressure (kgf mm^{-2})	Measured compliance at various locations (mm)								
	1	2	3	4	5	6	7	8	9
15	0.101	0.055	0.098	0.081	0.005	0.066	0.125	0.067	0.088
20	0.174	0.120	0.191	0.115	0.020	0.137	0.163	0.115	0.165
25	0.175	0.141	0.188	0.117	0.051	0.143	0.190	0.163	0.193
30	0.201	0.178	0.213	0.143	0.065	0.179	0.223	0.199	0.241

Fig. 10. (%) Error between the measured and simulated pressure values: (a) 15 kgf mm^{-2}; (b) 20 kgf mm^{-2}; (c) 25 kgf mm^{-2}; and (d) 30 kgf mm^{-2}.

Fig. 11. (%) Error between the measured and simulated compliance values: (a) 15 kgf mm^{-2}; (b) 20 kgf mm^{-2}; (c) 25 kgf mm^{-2}; and (d) 30 kgf mm^{-2}.

with the imprint mark of the flow field channel, indicating a lower interface contact resistance. The color at the circumference was darker than in the centre. When these two measured pressure contours were compared to the simulated contours of Fig. 5(a) and (b), the numerical model was reasonably accurate in predicting the actual cell assembly process.

Measured pressure values at nine local locations were extracted from the contours and are listed in Table 4. The compliance values of the gas diffusion layer at the same locations are listed in Table 5. The results of the trend were consistent with the numerical results of the values at the corner locations, 1, 3, 7, and 9 being larger and location 5 having the smallest value. However, they were not as definite due to manufacturing tolerances and process variations. As the assembly pressure increased, the results became more consistent.

5. Comparisons and discussion

Data from the numerical simulation were compared with those of the experimental measurement at specific locations of Fig. 8. The percentage error was calculated by the following equation:

$$(\%)\ \text{error} = \frac{\text{measured value} - \text{simulated value}}{\text{simulated value}} \times 100\%$$

The simulated data were taken as the datum because the numerical model was ideal. There were no tolerances, variations and uncertainties. At each set of analysis variables, the simulated results will be unique and repeatable. Hence, the (%) errors of the pressure values from Table 4 (measured pressure value) versus Table 2 (simulated pressure value) were computed and are listed in Fig. 10(a)–(d). Similarly, the (%) errors of the compliance values from Table 5 (measured compliance value) versus Table 3 (simulated compliance value) were computed and are listed in Fig. 11(a)–(d). First, the (%) error was within a range of 10–60%. The values were all in the same scale. The (%) errors, in general, were larger under a smaller assembly pressure. Second, the locations of maximum and minimum values were identical for all simulated versus measured results. Third, the pressure contours from the pressure films were almost identical to those of the numerical simulated results.

In the first stage of the cell assembly, the applied pressure was mostly to overcome the manufacturing tolerance and form errors of the fuel cell components, as listed in Table 1. As the assembly pressure increased, then, there was a stage where all the components were in elasticity deformation. After the assembly pressure exceeded the elasticity limit of some of the components, irreversible damage started to accumulate, and the characteristics of the pressure distribution and compliance became increasingly non-linear. Therefore, a cell may perform best at the second stage of cell assembly pressure.

6. Conclusions

The FEM analysis method was employed to simulate the cell stack assembly of a single cell with metallic bipolar plates. The physical properties and dimensions of the fuel cell components were collected with proper boundary condition assumptions, and actual loading conditions to establish the finite element model. The contours of pressure distribu-

tion and compliance were obtained for key components such as the MEA and gas diffusion layer. From these results, the effects of stack design and cell assembly procedures on stack integrity can be evaluated.

A single cell of the simulated FEM model was assembled in order to record measurement data for the purpose of comparison. The percentage errors of the pressure distribution of the gas diffusion layer, and the compliance of the gas diffusion layer were within 10–60%. These errors could be caused by:

1. manufacturing tolerance and form error of fuel cell components;
2. simplified static linear model;
3. measurement error from pressure film color to pressure distribution contour.

However, the trends of the pressure distribution, compliance and stresses were all very similar between the measurement and the simulation. Hence, the proposed numerical simulation model and procedures could be helpful in the evaluation of stack design and cell assembly.

The numerical simulation model and procedures could be extended to fuel cell stack design, to evaluate cell assembly parameters and to specify quality control specifications, allowing for the appropriate dimensions and tolerances of the cell components to be specified. The proper combinations of fuel cell components could be evaluated in advance in order to fulfill specific functional requirements, as well as to provide mechanical strength compatibility, thereby ensuring consistent and reliable cell performance in the future.

Acknowledgements

This research is funded by Ministry of Economic Affairs of Taiwan 91-EC-17-A-05-S1 -0012. The support from Yuan Ze fuel cell center is also greatly appreciated.

References

[1] W.K. Lee, C.H. Ho, J.W.V. Zee, M. Murthy, The effects of compression and gas diffusion layers on the performance of a PEM fuel cell, J. Power Sources 84 (1999) 45–51.
[2] H.S. Chu, C. Yeh, F. Chen, Effects of porosity change of gas diffuser on performance of proton exchange membrane fuel cell, J. Power Sources 123 (2003) 1–9.
[3] D. Chu, R. Jiang, Performance of polymer electrolyte membrane fuel cell PEMFC stacks, J. Power Sources 83 (1999) 128–133.
[4] S. Giddey, F.T. Ciacchi, S.P.S. Badwal, Design, assembly and operation of polymer electrolyte membrane fuel cell stacks to 1 kW capacity, J. Power Sources 125 (2004) 155–165.
[5] R. Jiang, D. Chu, Stack design and performance of polymer electrolyte membrane fuel cells, J. Power Sources 93 (2001) 25–31.
[6] B. Zhang, X. Wang, Y. Song, Pressurized endplates for uniform pressure distributions in PEM fuel cells, in: Proceeding of the First International Conference on Fuel Cell Development and Deployment.